Original article

Vwf K1362A resulted in failure of protein synthesis in mice

Naomi Sanda[1,2], Nobuaki Suzuki[3], Atsuo Suzuki[1], Takeshi Kanematsu[4], Mayuko Kishimoto[4], Hidetoshi Hasuwa[5], Akira Takagi[6], Tetsuhito Kojima[6], Tadashi Matsushita[3,4], Shigeo Nakamura[2]

[1]Department of Medical Technique, Nagoya University Hospital, Nagoya, Japan

[2]Department of Pathology and Clinical Laboratories, Nagoya University Graduate School of Medicine, Nagoya, Japan

[3]Department of Transfusion Medicine, Nagoya University Hospital, Nagoya, Japan

[4]Department of Clinical Laboratory, Nagoya University Hospital, Nagoya, Japan

[5]Department of Experimental Genome Research, Research Institute for Microbial Diseases, Osaka, Japan

Current address is Department of Molecular Biology Keio University School of Medicine, Tokyo, JAPAN

[6]Department of Pathophysiological Laboratory Sciences, Nagoya University Graduate School of Medicine, Nagoya, Japan

Running head: Analysis of *Vwf* K1363A knock-in mice

Correspondence to: Dr. Nobuaki Suzuki

Department of Transfusion Medicine

Nagoya University Hospital

65 Tsurumai-cho, Showa-ku, Nagoya, Aichi 466-0065, Japan

Tel: +81-52-744-2652; Fax: +81-52-744-2610

E-mail: suzukin@med.nagoya-u.ac.jp

Keywords: von Willebrand factor, mouse model, genetic mutation

Abstract

von Willebrand factor (VWF) is synthesized in megakaryocytes and endothelial cells (ECs), and has two main roles: to carry and protect coagulation factor VIII (FVIII) from degradation by forming VWF-FVIII complex; and to mediate platelet adhesion and aggregation at sites of vascular injury. Previous research using the HEK293 cell line revealed that the VWF K1362 mutation interacted directly with platelet glycoprotein Ib (GPIb). *Vwf* K1362A knock-in (KI) mice were therefore generated to verify the in vivo function of residue 1362 in binding to platelet GPIb. The Cre-loxP system was

employed to introduce the *Vwf* K1362A mutation systemically in mice. In blood coagulation analysis, the VWF antigen (VWF:Ag) of Lys1362Ala KI homozygous (homo) mice was below the sensitivity of detection by enzyme-linked immunosorbent assay. FVIII activities (FVIII:C) were 47.9±0.3% and 3.3±0.3% (K1362A heterozygous (hetero) and K1362A KI homo mice, respectively) compared to wild-type mice. Immunohistochemical staining analysis revealed that VWF protein did not exist in ECs of K1362A KI homo mice. These results indicated that VWF protein synthesis of K1362A was impaired after transcription in mice. K1362 seems to represent a very important position not only for VWF function, but also for VWF synthesis in mice.

Introduction

von Willebrand factor (VWF) is a multimeric glycoprotein that plays important roles in hemostasis and thrombosis. VWF is synthesized in megakaryocytes and endothelial cells (ECs). Since VWF synthesized in megakaryocytes is known to be stored in the alpha-granules of platelets, the main source of plasma VWF is ECs. VWF has two main roles: to carry and protect coagulation factor VIII (FVIII) from degradation by forming

VWF-FVIII complex; and to mediate platelet adhesion and aggregation at sites of vascular injury. Activation of the adhesive properties is induced in vivo upon the binding of VWF to subendothelial connective tissue, particularly under the conditions of high shear stress seen in the microcirculation. Activated VWF binds to the α chain of platelet glycoprotein Ib (GPIb) [1-3]. This interaction results in platelet adhesion, followed by platelet activation and aggregation. On the other hand, binding of VWF to GPIb in vitro can be induced by the antibiotic ristocetin, or by botrocetin, a snake venom protein. Ristocetin can bind both to GPIb and VWF [4], whereas botrocetin binds to VWF, but not GPIb [5, 6].

Matsushita et al. reported that several clustered mutations of charged residues within the VWF-A1 domain displayed reduced or increased function by clustered charged-to-alanine scanning mutagenesis [7]. Mutations within discontinuous segments including Glu1359-Arg1379, Arg1392-Arg1395, and Lys1405-Lys1408 decreased binding to GPIb, indicating that several residues within these segments may interact with GPIb. Based on the findings, they analyzed the contributions of 28 specific residues within the clusters of charged residues inside the VWF-A1 domain that were

involved in binding GPIb or botrocetin. Both ristocetin- and botrocetin-induced binding to GPIb were decreased by mutations at Lys1362, Arg1392, and Arg1395. In particular, Lys1362 was unique because ^{125}I-botrocetin binding remained despite impairment of the binding with ristocetin and botrocetin [8]. This result suggested that Lys1362 mutation interacts directly with GPIb. In this study, we established a mouse model of *Vwf* Lys1362Ala to analyze the in vivo function of residue 1362 in the binding to platelet GPIb.

Material and Methods

Construction of the *Vwf*-K1362A knock-in (KI) vector

To investigate the function of K1362A existing in the VWF A1 domain, we created a KI mouse. VWF K1362A targeting vector was created from exon 28 of the murine VWF gene by replacing a genomic fragment containing exon 28 of the K1362A mutation with a neo cassette. The K1362A mutation was introduced in the mouse gene using the targeting strategy outlined in Figure 1. The neo cassette provided positive and negative

selection, and genomic DNA from surviving clones was screened by Southern blot analysis.

A genomic DNA fragment containing murine VWF (C57BL/6J, Accession number NC__000072.6) was obtained by polymerase chain reaction (PCR) and used as a probe to isolate a genomic clone containing a segment of *Vwf* from a 129SVJ lambda FIX II genomic library (Stratagene, La Jolla, CA). The targeting vector (pNT1.1_Vwf-K1362A) was constructed from basic vector pNT1.1 [9]. The *Vwf* fragments consisted of a *Bgl*II/*Nco*I fragment (1.7 kb) as the 5' arm and a *Nco*I/GATC fragment (5.8 kb) as the 3' arm (Fig. 1A). We introduced the K1362A mutation into the 3' arm and an additional silent mutation to create a diagnostic *Bst*1107I site.

Generation of targeted mice

Linearized targeting vector was electroporated into D3 ES cells derived from 129Sv and screened for neomycin resistance. Two homologous recombinant ES clones were independently injected into C57BL/6J blastocysts to generate chimeric mice. Male chimera derived from one ES clone transmitted the recombinant allele to the next

generation (*Vwf*-K1362A). The loxP-neo cassette was removed by crossing the heterozygous mice with a CAG-Cre deleter mouse strain that constitutively expresses Cre recombinase to yield heterozygous KI (K1362A KI hetero) mice. K1362A KI homozygous (homo) mice were obtained from crossing K1362A KI hetero mice. PCR analysis was performed for genomic DNA isolated from tail biopsies obtained from wild-type (WT), R1362A KI hetero and homo mice. Long-range PCR was performed using a 5' external sense primer (5'-CAGCATGGGGTAGTGAACAA) and a 3' external antisense primer (5'-GTGACTGTAGCAGAAGGGAA), and (5'-CCTTCTATCGCCTTCTTGAC), followed by *Bst*1107I digestion to confirm the mutant. All research procedures involving animals were performed in accordance with the Laboratory Animals Welfare Act, the Guide for the Care and Use of Laboratory Animals, and the Guidelines and Policies for Rodent Experiments provided by the Institutional Animal Care and Use Committee (IACUC) at the Nagoya University Graduate School of Medicine and were reviewed and approved by the IACUC. The protocol was approved by the committee on the Ethics of Animal Experiments at Nagoya University Graduate School of Medicine (Permit Number: 09-04).

Blood sampling

Mice were anaesthetized deeply by sevoflurane, then whole blood was obtained by puncture of the inferior vena cava and collected into tubes with 3.2% sodium citrate (1 volume to 9 volumes of blood). Samples were centrifuged for 20 min at 3,000×*g* at room temperature to obtain platelet-poor plasma (PPP). All plasma samples were stored at -80°C until needed for analysis.

VWF antigen

Mouse VWF antigen (VWF:Ag) was determined by enzyme-linked immunosorbent assay (ELISA). Briefly, plates were coated with rabbit anti-human polyclonal VWF antibody (A0082; DAKO, Carpenteria, CA) overnight at 4°C. Plates were washed three times with PBS supplemented with 0.002% Tween 80. Standard samples and 1/25 diluted plasma samples (in PBS with 3% BSA) were applied to the coated plate for 2 h at room temperature with shaking. Plates were then washed four times with wash buffer. Bound VWF antigen was subsequently detected with horseradish peroxidase

(HRP)-conjugated rabbit anti-human VWF antibody (P0226, dilution 1/2000 in PBS with 3% BSA; DAKO), applied for 1 h at room temperature with shaking. After four washes, substrate buffer supplemented with 0.1 mg/mL ortho-phenylenediamine dihydrochloride (OPD) and 3 $\times 10^{-3}$% hydrogen peroxide were added to each well to colorimetrically detect HRP activity. After 10 min, the reaction was stopped with 50 µl of 2.5-M sulfuric acid and the plate was read at 492 nm in an ELISA microplate reader.

Measurement of FVIII activity

FVIII activity (FVIII:C) was measured by chromogenic assay (Chromogenix Coatest® SP FVIII; Sekisui Medical, Tokyo, Japan) according to the instructions from the manufacturer. The principle is as follows. In the presence of calcium and phospholipids, factor X is activated to factor Xa by factor IXa. This generation is greatly stimulated by FVIII, which may be considered as a cofactor in this reaction. By using optimal amounts of Ca^{2+} and phospholipids and an excess of factors IXa and X, the rate of activation of factor X is solely dependent on the amount of FVIII. Factor Xa hydrolyses the chromogenic substrate S-2765™, liberating a chromophoric group, pNA. The color

is then read photometrically at 405 nm. The standard curve was made using mouse standard plasma in this study.

Immunohistochemical staining

The organs, lung and heart were fixed in 4% paraformaldehyde for 7 days. Paraffin sections were made using a Young-type sliding microtome (Sakura Finetek, Tokyo, Japan) and a disposable microtome blade. Sections were approximately 3 mm in thickness and mounted on silane-coated slides. Immunohistochemical staining was performed according to the labeled streptavidin-biotin (LSAB) method. Deparaffinized sections were autoclaved at 120°C for 10 min to block endogenous peroxidase activity, then incubated sequentially at 4°C for 1 h with rabbit anti-human polyclonal VWF antibody (A0082; DAKO), diluted to 1:100 in Tris-buffered saline (TBS) and incubated in streptavidin-biotin-peroxidase solution according to the instructions for the LSAB-kit (DAKO). The immunoreaction was visualized by peroxidase-diaminobenzidine (DAB) reaction. Sections were finally counterstained with hematoxylin.

Stained sections were then observed under light microscopy (DP70; Olympus, Tokyo,

Japan).

Results

Genetic analysis of VWF K1362A mice

Southern blot and PCR analyses confirmed correct homologous recombination of ES cells (Figs. 1E, 2B, C). DNA analysis of mice was performed using DNA from tail tissue.

RNA was analyzed from the heart, liver and lung of WT and knockout (KO) K1362A homo mice. Relative expression of lung RNA was 60% in K1362A KI homo mice and 7% in KO mice compared with WT mice (Fig. 3A). *Vwf* mRNA was identified in heart, liver and lung of K1362A KI homo mice as well as WT mice by RT-PCR (Fig. 3B). On the other hand, a quantitative real time PCR analysis indicated RNA expressions were extremely low from the heart and liver both in K1362A homo and WT mice (data not shown). The cDNA was generated from heart, liver and lung mRNA and sequence analysis confirmed that the intended mutation was introduced in K1362A, but not in WT (Fig. 3C).

VWF and FVIII measurement by plasma

VWF antigen levels in plasma were analyzed using ELISA. VWF antigen of K1362A KI homo and KO mice were <1.6% (Table 1). FVIII:C was 2.3%±0.1%, 47.9±0.3% and 3.3±0.3% in VWF KO, K1362A hetero and K1362A KI homo mice, respectively, compared to WT mice (Table 1).

Immunohistochemical staining analysis of VWF in endothelial cells (ECs)

VWF immunostaining was performed using heart and lung tissues from WT and K1362A homo mice. In heart, VWF was not detected in WT or K1362A homo mice (data not shown). In lung, expression of VWF was observed in ECs of WT mice, but not in K1362A homo mice (Fig. 4).

Discussion

A previous study identified that K1362A mutant was unique, in a binding experiment with platelet glycoprotein Ibα (GPIbα) or botrocetin [8], since the binding to botrocetin

was normal, but binding to GPIbα was completely abolished both in the presence of ristocetin or botrocetin.

In the crystal structure of the complex of human VWF-A1 and the N-terminal fragment of GPIbα, leucine-rich repeats (LRR) 5 to 8 and the COOH-terminal flank region known as the β-switch of GPIbα interact with A1 helix α3, loop α3β4, and strand β3 [10]. K1362 is located on helix α3, near the β-switch of GP1bα (Fig. 5A). Changing lysine to alanine is expected to shorten the side chains (4-aminobutyl group) involved in binding (Fig. 5B) and is supposed to abolish the binding.

As further research into the interaction between VWF and GP1bα, K1362A KI mice were generated and subjected to evaluation of the influence on interaction with GP1bα. Mouse models so far have drawn a great deal of attention, offering ideal tools to study the in vivo function of VWF [11, 12]. As the structure of the VWF-A1 domain shows high homology between human and mice, mutations would likely have similar effects.

K1362A KI mice were prepared and PCR was carried out to confirm inclusion of the K1362A mutation. In the relative mRNA quantification of VWF, the expression level was approximately 60% compared with WT mice, which was deemed adequate to

synthesize VWF protein. However, mature VWF antigen was not observed by ELISA of plasma. VWF is known to be synthesized in ECs and secreted into plasma. ECs from heart, liver and lung tissue were thus subjected to immunostaining to confirm the existence of VWF antigen in ECs. Although ECs from the lungs of WT mice contained VWF antigen, those of K1362A KI homo mice did not (Fig. 4). These data indicate that the K1362A mutation resulted in the abolishment of processing after transcription.

In an expression system using human kidney 293T cells, expression of human VWF K1362A was clearly observed. Tertiary structural models of human and mouse A1 domains were created and compared using Pymol (PDB: 1AUQ [13] 1U0O [6], and appeared extremely similar (Fig. 5C, D). The structure of the mouse K1362A mutation was modeled using SWISS-MODEL software (https://swissmodel.expasy.org/) and the structure was compared to simulated WT on a Pymol-created model (Fig. 6). The single amino acid change from Lys to Ala shortened the amino acid side chain (Fig. 6A, B), and a small hole was formed on the protein surface (Fig. 6C, D). In the human case, this change did not alter the protein expression, but in mouse A1 domain, the K1362A missense mutation was speculated to result in the loss of the positively charged Lys

4-aminobutyl group and may thus have an unexpected impact on the protein structure. The structural model could expect the A1 tertial structure, but VWF is multimeric and the mouse mutation was also suggested to affect the multimeric superstructure. The predicted surface charge of the mutated region (Fig. 6C, D) may resulted in loss of protein expression in full-length recombinant VWF.

In an experiment using human VWF cDNA, K1362A was well expressed without binding to GPIb. Considering that no reports have described natural human K1362A mutation leading to development of type1/3 von Willebrand disease, an effect on the protein structure/expression might only be seen in mice. However, limited information is obtained by Hommais A et al. who described a mutation to tyrosine at VWF Lys1362, K1362T (c.4085 A>C) [14]. They showed recombinant T1362 VWF (T1362rVWF) expressed from COS-7 cells had no significant effect on secretion or multimerization or FVIII binding, but T1362rVWF exhibited significantly decreased ristocetin- and botrocetin-induced binding to GPIb, that is compatible with our previous finding observed in recombinant VWF K1362A [14]. The phenomenon we observed is extremely unusual and further structural interpretation using multimeric VWF model is

required.

Conflict of interest

This research was supported by JSPS KAKENHI Grant Number JP 22591059 and Novartis Research Grants.

Acknowledgement

We would like to thank NPO Biotechnology Research and Development for technical assistance. We wish to thank the staff of the Division of Experimental Animals at Nagoya University Graduate School of Medicine for their technical support. We are also grateful to Kimiko Sannoudo for obtaining blood from mice and PCR typing.

References

1. Handa M, Titani K, Holland LZ, Roberts JR, Ruggeri ZM. The von Willebrand factor-binding domain of platelet membrane glycoprotein Ib. Characterization by monoclonal antibodies and partial amino acid sequence analysis of proteolytic fragments. *The Journal of biological chemistry* 1986; **261:** 12579-85.

2. Vicente V, Houghten RA, Ruggeri ZM. Identification of a site in the alpha

chain of platelet glycoprotein Ib that participates in von Willebrand factor binding. *The Journal of biological chemistry* 1990; **265:** 274-80.

3. Murata M, Ware J, Ruggeri ZM. Site-directed mutagenesis of a soluble recombinant fragment of platelet glycoprotein Ib alpha demonstrating negatively charged residues involved in von Willebrand factor binding. *The Journal of biological chemistry* 1991; **266:** 15474-80.

4. Scott JP, Montgomery RR, Retzinger GS. Dimeric ristocetin flocculates proteins, binds to platelets, and mediates von Willebrand factor-dependent agglutination of platelets. *The Journal of biological chemistry* 1991; **266:** 8149-55.

5. Andrews RK, Booth WJ, Gorman JJ, Castaldi PA, Berndt MC. Purification of botrocetin from Bothrops jararaca venom. Analysis of the botrocetin-mediated interaction between von Willebrand factor and the human platelet membrane glycoprotein Ib-IX complex. *Biochemistry* 1989; **28:** 8317-26.

6. Fukuda K, Doggett T, Laurenzi IJ, Liddington RC, Diacovo TG. The snake venom protein botrocetin acts as a biological brace to promote dysfunctional platelet aggregation. *Nature structural & molecular biology* 2005; **12:** 152-9.

7. Matsushita T, Sadler JE. Identification of amino acid residues essential for von Willebrand factor binding to platelet glycoprotein Ib. Charged-to-alanine scanning mutagenesis of the A1 domain of human von Willebrand factor. *The Journal of biological chemistry* 1995; **270:** 13406-14.

8. Matsushita T, Meyer D, Sadler JE. Localization of von willebrand factor-binding sites for platelet glycoprotein Ib and botrocetin by charged-to-alanine scanning mutagenesis. *The Journal of biological chemistry* 2000; **275:** 11044-9.

9. Inoue N, Ikawa M, Isotani A, Okabe M. The immunoglobulin superfamily protein Izumo is required for sperm to fuse with eggs. *Nature* 2005; **434:** 234-8.

10. Huizinga EG, Tsuji S, Romijn RA, Schiphorst ME, de Groot PG, Sixma JJ, *et al.* Structures of glycoprotein Ibalpha and its complex with von Willebrand factor A1 domain. *Science (New York, NY)* 2002; **297:** 1176-9.

11. Pendu R, Christophe OD, Denis CV. Mouse models of von Willebrand disease. *Journal of thrombosis and haemostasis : JTH* 2009; **7 Suppl 1:** 61-4.

12. Chen J, Zhou H, Diacovo A, Zheng XL, Emsley J, Diacovo TG. Exploiting the kinetic interplay between GPIbalpha-VWF binding interfaces to regulate hemostasis

and thrombosis. *Blood* 2014; **124:** 3799-807.

13. Emsley J, Cruz M, Handin R, Liddington R. Crystal structure of the von Willebrand Factor A1 domain and implications for the binding of platelet glycoprotein Ib. *The Journal of biological chemistry* 1998; **273:** 10396-401.

14. Hommais A, Stépanian A, Fressinaud E, Mazurier C, Meyer D, Girma JP, et al. Mutations C1157F and C1234W of von Willebrand factor cause intracellular retention with defective multimerization and secretion. *The Journal of Thrombosis and Hemostasis* 2006; **4:** 148-57.

Figure legends

Fig. 1. Knock-in strategy for *Vwf K1362A* mice

(A) *Vwf* fragments consisted of a *Bgl*II/*Nco*I fragment (1.7 kb) as the 5' arm and a *Nco*I/GATC fragment (5.8 kb) as the 3' arm.

(B) The targeting vector (pNT1.1_Vwf-K1362A) was constructed from basic vector pNT1.1 [9]. It was created from exon 28 of the murine VWF gene by replacing a genomic fragment containing exon 28 of K1362A mutation with neo cassette.

(C) To generate chimeric mice, the targeting vector was electroporated into D3 ES cells derived from 129Sv and screened for neomycin resistance.

(D) The loxP-neo cassette was removed by crossing with a CAG-Cre deleter mouse strain that constitutively expressed Cre recombinase.

(E) Correct homologous recombination or Cre-mediated excitation was confirmed by Southern blot analysis (Fig. 2) or analyzing long-PCR products from ES cells.

Fig. 2. Southern blotting analysis of ES clones

(A) Fragment size: *Sac* I WT: 3718 bp; K1362A: 5462 bp; *Eco*RI WT: short arm side 13,728 bp, long arm side 13,728 bp; K1362A: short arm side 6868 bp, long arm side 8604 bp

(B) Southern blotting analysis of 5' short arm side. Lanes 1-6 are heterozygous K1362A and 7 is WT.

(C) Southern blotting analysis of 3' long arm side. Lanes 1-6 are heterozygous K1362A and 7 is WT.

VWF: von Willebrand factor; WT: wild type

Fig. 3. Analysis of *Vwf* gene transcription

(A) Relative expression of *Vwf* mRNA by real-time PCR. The relative levels of *Vwf* mRNA from lung were 7% and 60% (*Vwf* KO and K1362A, respectively)

(B) The result of RT-PCR demonstrated the expression of *Vwf* mRNA in heart, liver and lung from K1362A, as well as WT.

(C) The cDNA sequence analyses of WT and K1362A were confirmed. To generate K1362A, two codons were replaced, A->G and A->C. An additional silent mutation to create a diagnostic *Bst*1107I site was also introduced, C->T. These intended mutations were correctly introduced.

WT: wild-type mice, VWF KO: von Willebrand factor knock-out mice, K1362A: K1362A knock-in homo mice, RT:Reverse Transcription

Fig. 4. Immunohistochemical staining analysis of ECs from lung tissue

(A) Arrows show VWF in ECs.

(B) VWF was not detected in K1362A KI homo mice.

WT: wild type; K1362A KI: K1362A knock-in; ECs: endothelial cells; VWF: von Willebrand factor

Fig. 5. Overall structure of VWF-A1 domain

(A, B) Binding structure model of the human VWF-A1 domain and GPIbα complex (PDB: 1SQ0). A ribbon representation of the VWF A1 domain is colored green, and GPIbα is colored pink. (A) is WT and (B) is K1362A simulated model of the VWF A1 domain. The K (Lys) 1362 residue is shown in blue (A), and the A (Ala) residue is shown in red (B).

(C) Human VWF-A1 domain structure is colored green (PDB:1AUQ) and K1362 residue is colored blue.

(D) Mouse VWF-A1 domain structure is colored orange (PDB: 1U0O) and K1362 residue is colored blue.

Fig. 6. Structural change simulation for mouse VWF-A1 domain

(A, B) Mouse VWF-A1 domain structure is colored green (PDB: 1U0O), (A) is WT and

(B) is K1362A simulated model. The K1362 residue is shown in blue (A), and the A1362 residue is shown in pink (B).

(C, D) Surface charge distribution map of mouse VWF-A1 domain, (C) is WT and (D) is K1362A simulated model.

Table

1

	VWF antigen (VWF:Ag)	FVIII activity (FVIII:C)
VWF knockout	<1.6%	2.3±0.1%
VWF K1362A KI hetero	12.3±3.4%	47.9±0.3%
VWF K1362A KI homo	<1.6%	3.3±0.3%

2 Table 1. The level of VWF antigen and FVIII activity in VWF KO, VWF K1362A KI

3 hetero and homo mice compared with wild type (WT) mice.

Figure 1

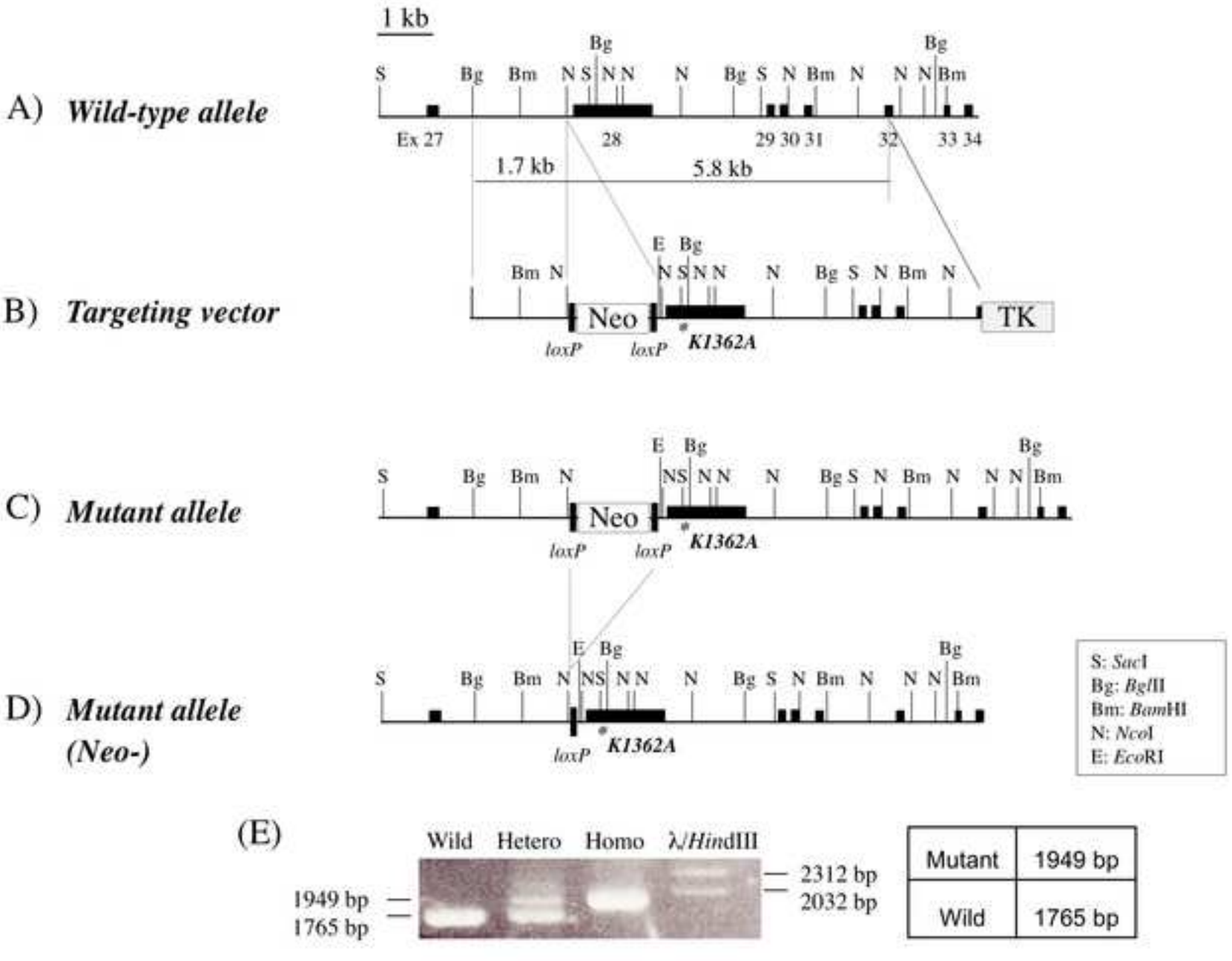

Figure 2

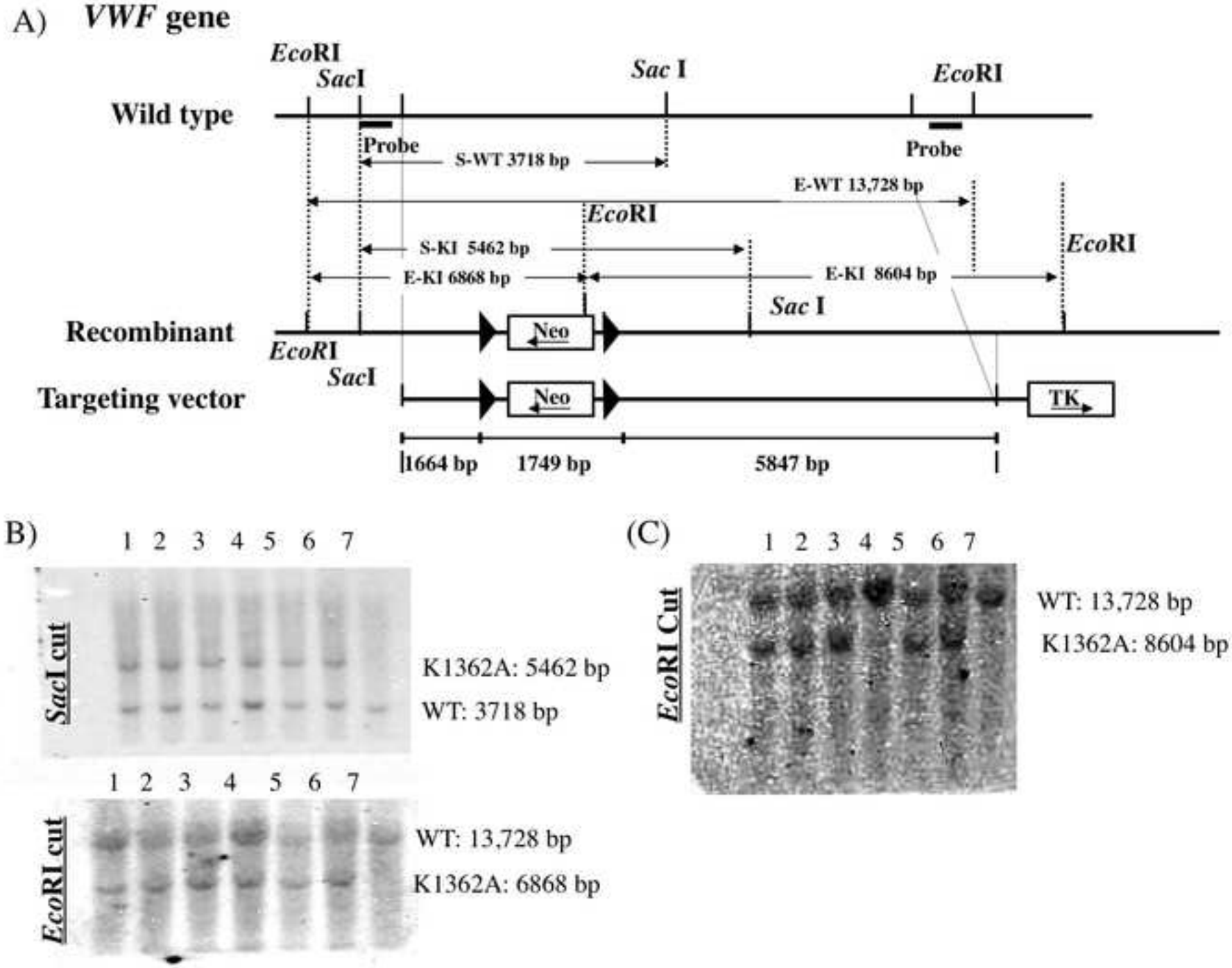

Figure 4

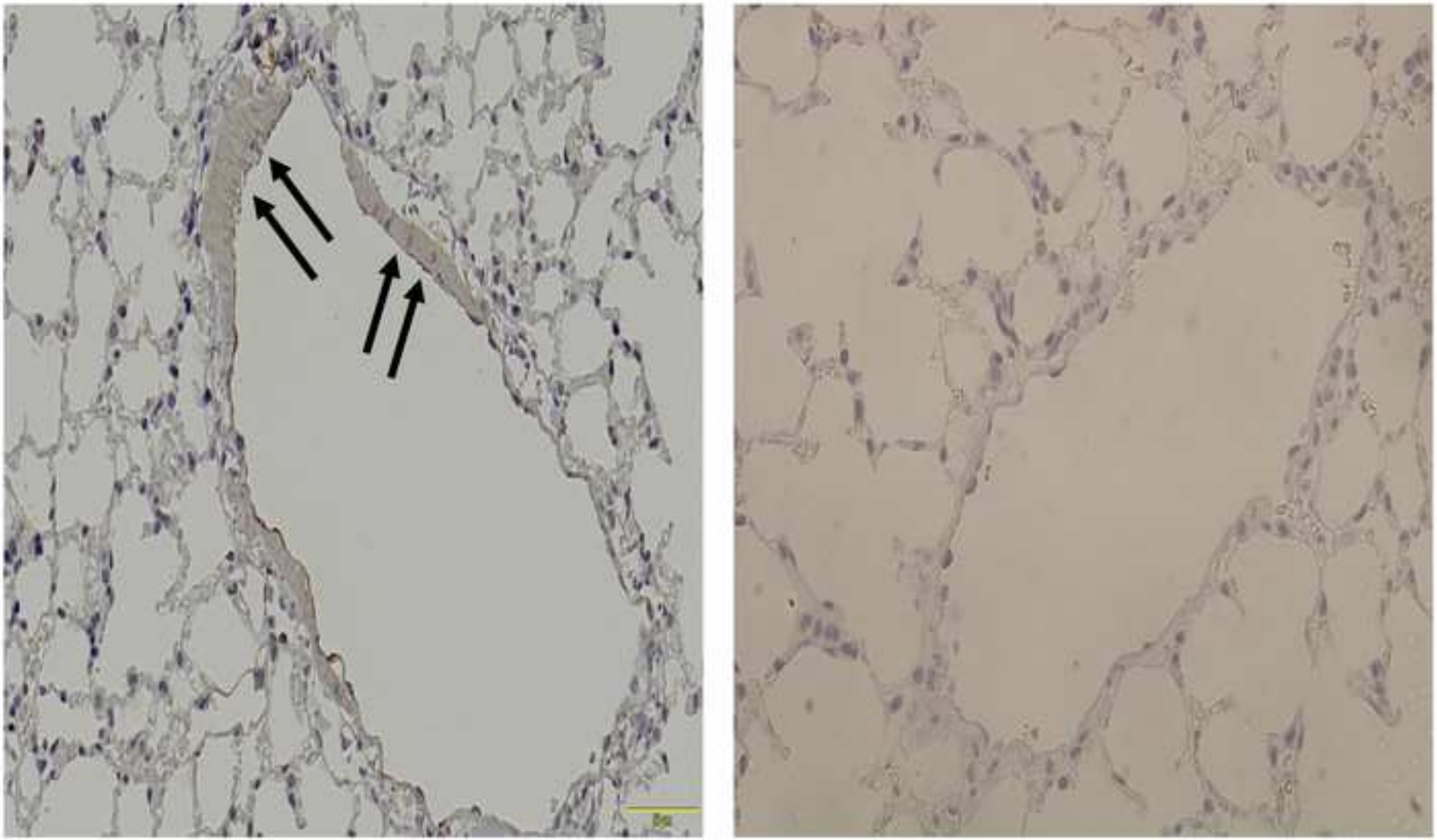

A) WT

B) K1362A

Figure 5

Click here to download Figure renamed_17d0b.jpg

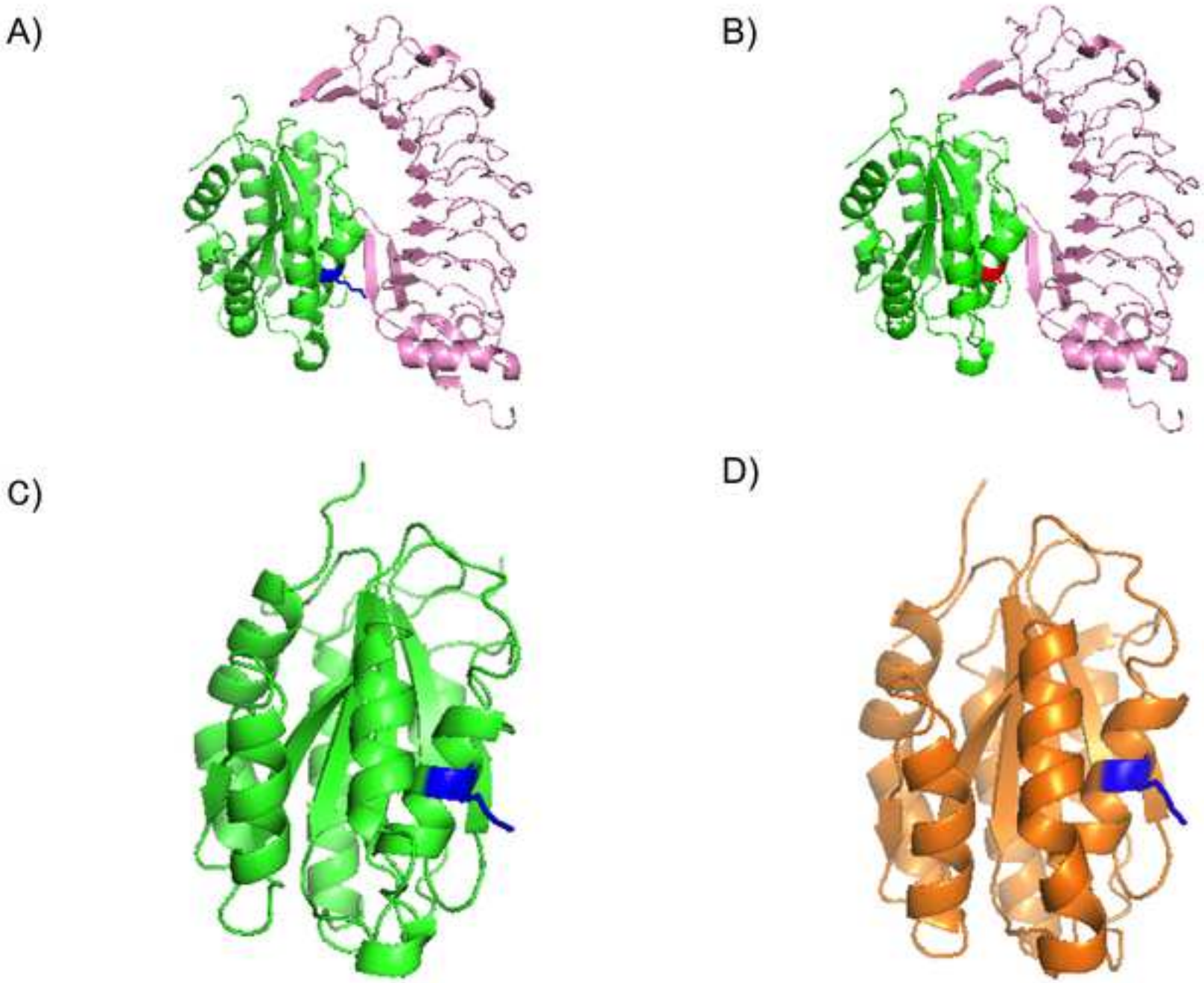

Figure 6

Click here to download Figure renamed_2ace1.jpg

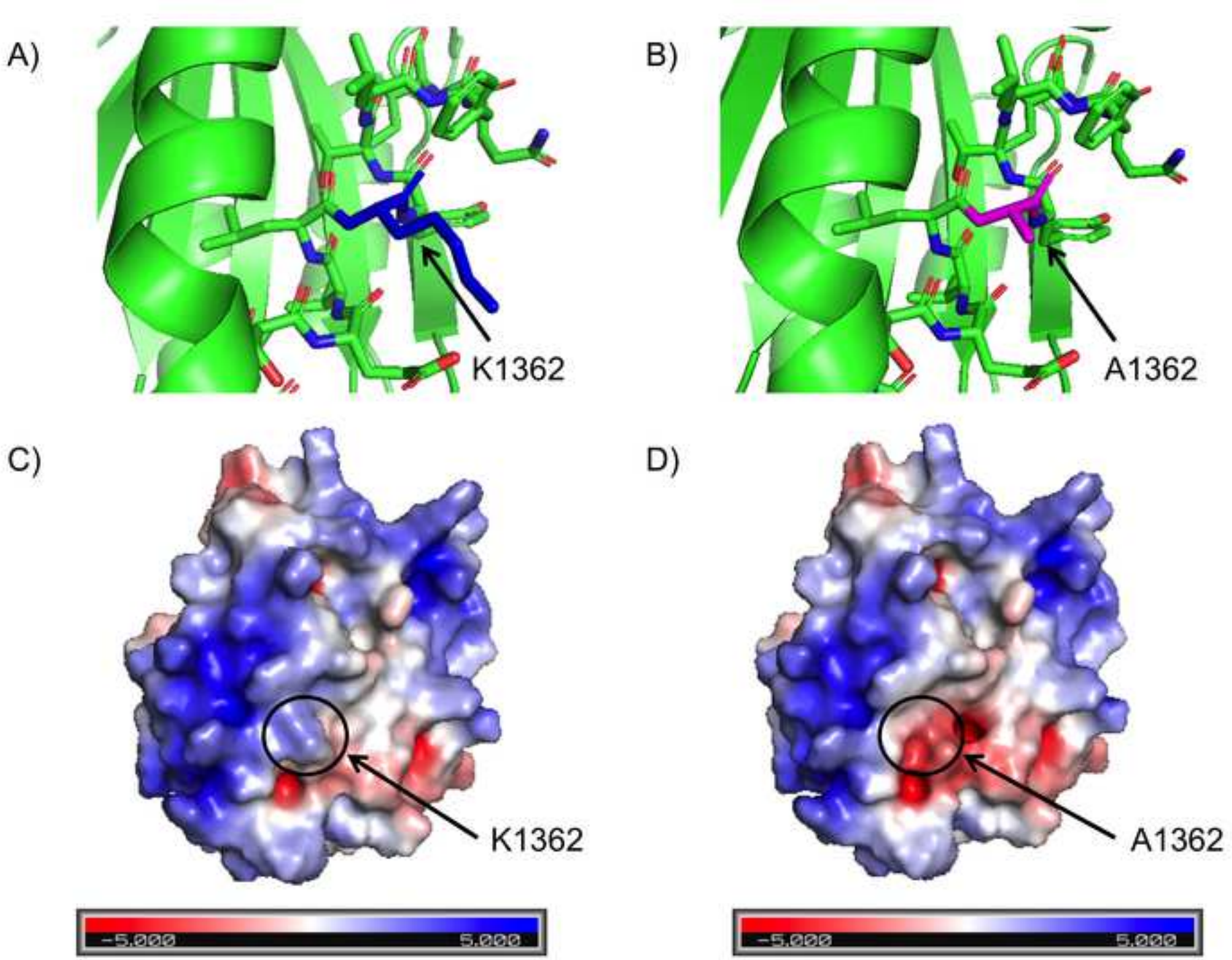

Figure 3